Mixed Reality and Deep Learning for External Ventricular Drainage Placement: A Fast and Automatic Workflow for Emergency Treatments

Maria Chiara Palumbo[1(✉)], Simone Saitta[1], Marco Schiariti[2], Maria Chiara Sbarra[1], Eleonora Turconi[1], Gabriella Raccuia[2], Junling Fu[1], Villiam Dallolio[3], Paolo Ferroli[2], Emiliano Votta[1], Elena De Momi[1], and Alberto Redaelli[1]

[1] Department of Electronics Information and Bioengineering, Politecnico Di Milano, Milan, Italy
mariachiara.palumbo@polimi.it
[2] Department of Neurosurgery, Carlo Besta Neurological Institute IRCCS Foundation, Milan, Italy
[3] Promev SRL, Lecco, Italy

Abstract. The treatment of hydrocephalus is based on anatomical landmarks to guide the insertion of an External Ventricular Drain (EVD). This procedure can benefit from the adoption of Mixed Reality (MR) technology. In this study, we assess the feasibility of a fully automatic MR and deep learning-based workflow to support emergency EVD placement, for which CT images are available and a fast and automatic workflow is needed. The proposed study provides a tool to automatically i) segment the skull, face skin, ventricles and Foramen of Monro from CT scans; ii) import the segmented model in the MR application; iii) register holograms on the patient's head via a marker-less approach. An ad-hoc evaluation approach including 3D-printed anatomical structures was developed to quantitatively assess the accuracy and usability of the registration workflow.

Keywords: Mixed reality · Deep learning · External ventricular drainage

1 Introduction

External Ventricular Drainage (EVD) represents the optimal surgical treatment for emergency cases of hydrocephalus [1]. This procedure consists in draining

M.C. Palumbo and S. Saitta—Equal first authorship.

Supplementary Information The online version contains supplementary material available at https://doi.org/10.1007/978-3-031-16449-1_15.

L. Wang (Eds.): MICCAI 2022, LNCS 13437, pp. 147–156, 2022.
https://doi.org/10.1007/978-3-031-16449-1_15

cerebrospinal fluid by inserting a catheter into the brain ventricles, positioning the tip on the Foramen of Monro (FoM). EVD placement is usually performed blindly, relying on paradigmatic anatomical landmarks localized freehand on the patient's head, thus carrying the risk of catheter malpositioning that can lead to hemorrhage, infections, brain tissue damage, multiple passes and reinsertion, entailing unnecessary brain trauma. Despite being a relatively simple procedure, a nearly 50% inaccuracy rate has been reported [1]. To address these issues, pre-operative images can provide helpful guidance during EVD placement and insertion [1,16], for instance, when combined with neuronavigation systems [10]. However, the high cost and significant encumbrance of these systems makes them hard to be adopted in the operating room. Mixed Reality (MR)-based solutions can represent a low-cost, easily portable guidance system for EVD placement. Previous studies have shown the feasibility of adopting MR based solutions for ventriculostomy procedures, providing visualization of internal brain structures [5], or to register the manually segmented holographic content on the patient's anatomy using marker based methods [3,9,13]. Nonetheless, these approaches do not represent adequate solutions for emergency cases where both automatic segmentation and quick registration need to coexist in a fast multistep routine. A first attempt to superimpose holograms on real world object using HoloLens2 Head Mounted Display (HMD) (Microsoft, Redmond, WA) and its depth camera via a marker-less approach, has been reported [7], resulting in low accuracy. The goal of this study was to assess the feasibility and accuracy of a MR and deep learning-based workflow to support EVD placement, in emergency procedures for which preoperative CT images are only available and a fast and automatic workflow is critical. The proposed study provides a tool to automatically i) segment the skull, skin, ventricles and FoM from computed tomography (CT) scans; ii) import the segmented model in the MR application; iii) register holograms on the patient's head via a marker-less approach.

2 Methods

The envisioned surgical workflow graphically depicted in Fig. 1 is divided into consecutive steps resulting in a final MR application specifically tailored for HoloLens2 (H2) device. The following sections provide a detailed description on the development of the automatic segmentation (Sect. 2.1), automatic registration (Sect. 2.2) and registration accuracy assessment (Sect. 2.3) methods.

2.1 Automatic Segmentation

3D CT scans of 200 subjects (including 41 cases of hydrocephalus) acquired between 2018 and 2022 were used as benchmark (pixel spacing ranging from 0.543×0.543 to $0.625 \times 0.625\,\text{mm}^2$, slice thickness between 0.625 and 1.25 mm). The study was approved by the local ethical committee and informed consent was waived because of the retrospective nature of the study and the analysis of anonymized data.

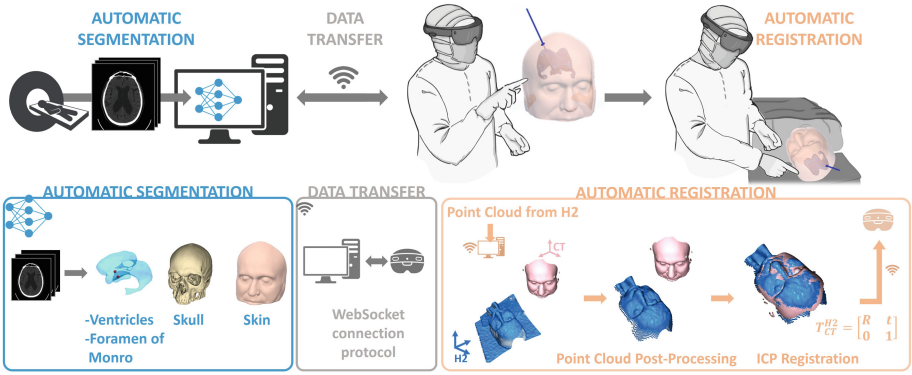

Fig. 1. Schematic representation of the developed workflow: the 3D CT images are automatically segmented to obtain the brain structures that will be sent to H2 device through an internet connection protocol. The user is then able to visualize the holographic models and set a path between the FoM and an entry point on the skin layer. The point cloud (PtC) of the skin surface of the patient is acquired using H2 depth camera and this data is used to estimate the transformation matrix $\mathbf{T}_{CT}^{H2}$.

Skin and Skull Segmentation was performed through i) automatic elimination of the mouth region in case of dental implant inducing artifacts; ii) thresholding (bone tissue: high-pass filter, threshold of 500 Hounsfield units (HU) [11]; skin: band-pass filter, lower and upper thresholds of -100 HU and 50 HU, respectively); iii) hole filling and smoothing.

Ventricle Segmentation was performed by a neural network (NN) based on a 3D UNET architecture, composed of an input layer of 16 filters, encoder and decoder branches of 5 resolution levels each, a bottleneck block and skip connections via concatenation [14]. The NN was trained and tested using all the CT volumes: the two lateral ventricles and the third ventricle were manually segmented by two experienced operators, guaranteeing that each acquisition was segmented by at least one user. The whole dataset was divided into training and test sets: 180 (90%) scans with their corresponding ground truth segmentations were randomly selected and used for NN training. A data augmentation routine was implemented to increase dataset diversity. Random rotations, mirroring and affine transformations were applied to the processed patches. A combination of Lovasz-Softmax loss and focal loss [12] was used to trained the NN to perform simultaneous segmentation of the lateral and third ventricles. The remaining 20 scans (10%), including 5 cases of hydrocephalus, were used for testing.

Detection of Foramen of Monro, which is the target for the tip of the catheter during EVD, was performed by a recursive thresholding approach [12].

2.2 Automatic Registration

The registration process was conceived to allow the end user to reliably superimpose the MR representation of the segmented skin model ($\mathcal{S}_{CT}$) on the head

of the real patient, whose face is acquired as a 3D point cloud (PtC) using the H2 depth sensing camera. This step was conceived to be performed before any surgical draping, once the position of the head is already fixed for the entire duration of the procedure. The holographic interface that permits the surgeon to acquire the 3D PtC and then run the registration algorithm, was designed in Unity3D (Unity Technologies, version 2020.3.1LTS) using the MR toolkit library MRTK v2.7.0. The algorithm consisted of the following steps (Fig. 2):

- Acquire the PtC of the facing surface $\{\boldsymbol{p}_{i,H2}\}$, using H2 research mode [15], and the position of the H2 device itself ($\boldsymbol{p}_{camera,H2}$), both referred to the H2 global coordinate reference system.
- Initialize the position of $\mathcal{S}_{CT}$ with respect to the target $\{\boldsymbol{p}_{i,H2}\}$ based on $\boldsymbol{p}_{camera,H2}$.
- Apply an Hidden Point Removal algorithm [8] to $\mathcal{S}_{CT}$ to filter out points in the back of the head to avoid unnecessary computations.
- Extract $\{\boldsymbol{p}_{i,H2}\}$ points belonging to the face through a DBSCAN density based clustering algorithm [6].
- Apply a Fast Global Registration algorithm [17] between the simplified $\mathcal{S}_{CT}$ and the cleaned $\{\boldsymbol{p}_{i,H2}\}$, obtaining a first alignment, which is then refined via Local Refined Registration method based on a Point-to-Plane iterative closest point (ICP) algorithm [4] to obtain $\mathbf{T}_{CT}^{H2}$. All the described steps related to the PtC tweaking and registration were implemented using the open3D library [18].
- Send back $\mathbf{T}_{CT}^{H2}$ to H2 and apply it to the holographic model of $\mathcal{S}_{CT}$, thus allowing the surgeon to visualize the segmented model aligned with the patient face $\mathcal{S}_{H2} = \mathbf{T}_{CT}^{H2}\mathcal{S}_{CT}$.

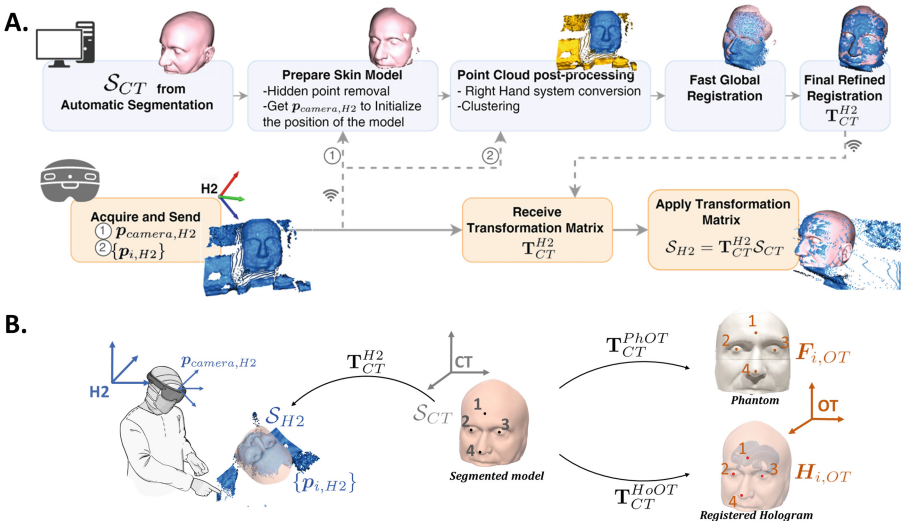

Fig. 2. A. Detailed representation of the registration workflow for the MR environment with B. The considered coordinate systems and transformation matrices.

2.3 Registration Accuracy Assessment

An experimental setup to evaluate the automatic registration accuracy was developed (Fig. 3A). The evaluation was divided into two different procedures to evaluate: 1. the accuracy of the hologram-to-phantom registration; 2. the targeting accuracy in a ventriculostomy-like procedure. For both tests, a 3D model of a patient with hydrocephalus was reconstructed from automated CT scan segmentation. The extracted skin model was modified to add four markers consisting in conical cavities on the skin surface at the left eye, right eye, nose and forehead, respectively. The modified model was 3D-printed and used to simulate a real patient's head. An optical tracker (OT) system (NDI Polaris Vicra) equipped with a trackable probe was used to acquire the position of the conical markers on the phantom, designed to accommodate the tip in a unique manner. The position of the markers was also reported in the holographic model where four red spheres of 1 mm of diameter were added to highlight each marker position.

To evaluate the accuracy of the hologram-to-phantom registration, an H2 expert user was asked to repeat the following procedure 10 times:

- Acquire the 4 markers position on the printed phantom in the OT space ($\boldsymbol{F}_{i,OT}$, with $i = 1, ..4$) (Fig. 3B).
- Wearing the H2 device execute the automatic registration and then, moving away the phantom, place the tip of the probe in correspondence of the 4 holographic marker to obtain their positions in the OT space ($\boldsymbol{H}_{i,OT}$, with $i = 1, ..4$). For this phase the probe is attached to a tripod which stabilizes the probe movement not limiting its orientation in the space (Fig. 3C).

The distance between the phantom and holographic model was assessed both by computing the Euclidean distance $e_{ij} = ||\boldsymbol{F}_{ij,OT} - \boldsymbol{H}_{ij,OT}||$ of the $i-th$ marker

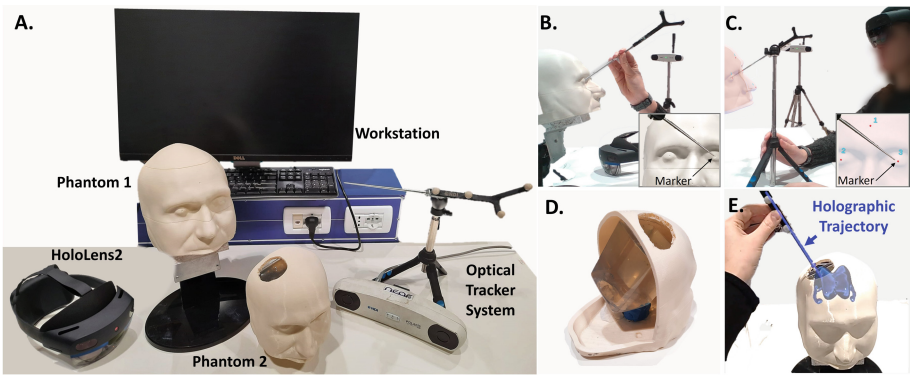

Fig. 3. A. Experimental setup showing the hardware and physical components needed to test the registration accuracy; user executing the first test is evaluating the position of the 4 marker on the printed phantom B., and on the registered holographic model C.; D. phantom used by neurosurgeons for the second test while E. trying to insert the OT probe to match the holographic trajectory.

and $j-th$ coordinate (x, y, z), but also providing an estimate of the error for each point of the skin surface and ventricle. To do this, a first transformation matrix $\mathbf{T}_{CT}^{PhOT}$ was computed to map $\mathcal{S}_{CT}$ with the 4 markers of the printed phantom $\boldsymbol{F}_{i,OT}$, and a second one $\mathbf{T}_{CT}^{HoOT}$ to map $\mathcal{S}_{CT}$ with the 4 markers of the registered hologram $\boldsymbol{H}_{i,OT}$ (Fig. 2B). A least-square solution based on the singular value decomposition algorithm [2] was applied to compute the transformation matrices. Finally, the point-to-point distance d_j with $j = 1, ..N$ vertices, was computed as:

$$d_j = ||\mathbf{T}_{CT}^{PhOT}\boldsymbol{m}_{j,CT} - \mathbf{T}_{CT}^{HoOT}\boldsymbol{m}_{j,CT}|| \tag{1}$$

with $\boldsymbol{m}_{j,CT}$ being the vertices of the segmented model of the skin and ventricles in the CT space. The root mean square error ($RMSE$) was computed as:

$$RMSE = \sqrt{\frac{1}{N}\Sigma_{j=1}^{N} d_j^2} \tag{2}$$

To evaluate targeting accuracy, another phantom was 3D-printed from the same segmented model, provided with a large hole in proximity of a common entry point for a ventriculostomy procedure and with an internal box full of gelatin mimicking brain tissue (6% gelatin in water) (Fig. 3D). A membrane was placed on top of the hole entrance to reduce the bias experienced by the users when choosing the point of entrance. For this test, 7 experienced neurosurgeons were asked to:

- acquire the positions of the 4 conical markers on the phantom with the OT probe $\boldsymbol{F}_{i,OT}$.
- do a blind (i.e., without wearing the H2) ventriculostomy procedure using the OT probe as a catheter, trying to reach the FoM based on anatomical references. Once deemed arrived to the target, the tip position of the probe was acquired in the OT space ($\boldsymbol{p}_{blind,OT}$)
- wear the H2 in which the segmented model is visualized to perform a registration procedure on the phantom annotating $\mathbf{T}_{CT}^{H2}$.
- guided by the visualization of an holographic path that goes from the skin to the FoM, insert the probe and try matching the holographic trajectory (Fig. 3E). Again, once the FoM was deemed reached, the position of the probe in the OT space was acquired ($\boldsymbol{p}_{Hguided,OT}$).

The transformation matrix $\mathbf{T}_{CT}^{PhOT}$ was computed to refer the position of the inserted probe to the internal structures of the brain, thus evaluating the tip position in the blind and hologram guided procedure. To quantify the improvement brought by adopting the proposed methodology, 7 neurosurgeons independently simulated EVD procedures on the gelatin phantom. Of note, none of the participant was familiar with the mixed reality device. The targeting accuracy improvement was computed as: $\Delta_{\%} = \left(\frac{|\boldsymbol{p}_{blind,OT} - \boldsymbol{p}_{Hguided,OT}|}{|\boldsymbol{p}_{blind,OT} - \boldsymbol{p}_{t,OT}|} \times 100\right)\%$, where $\boldsymbol{p}_{t,OT}$ is the target position in OT space.

3 Results

3.1 Automatic Segmentation

Brain Ventricles Test Set Results. The trained NN was applied to run inference on the test set made of 20 CT scans, 5 of which presented hydrocephalus. Our automatic segmentation algorithm was able to generalize to new cases, extracting the 3D ventricle regions with accuracy (Fig. 4), requiring approximately 130 s per scan. For the lateral ventricles, mean Dice score and 95% Hausdorff distance were equal to of 0.88 and 14.4 mm, respectively. For the third ventricle, mean Dice score and 95% Hausdorff distance were equal to 0.62 and 19.4 mm. Considering the five test cases with hydrocephalus, a mean Dice score of 0.94 was obtained for the lateral ventricles and a mean value of 0.81 for the third ventricles, while 95% Hausdorff distances were equal to 18.3 mm and 7.48 mm, respectively.

For all test cases with hydrocephalus, the ventricle surface reconstruction accuracy was sufficient to automatically detect the FoM.

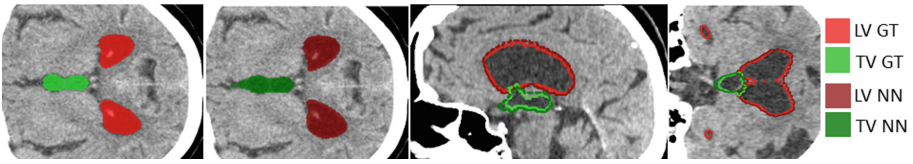

Fig. 4. Comparison of manual (ground truth, GT) segmentation in bright red (lateral ventricles, LV) and bright green (third ventricle, TV), vs. automatic segmentation obtained by the trained neural network (NN) in dark red (lateral ventricles, LV) and dark green (third ventricle, TV) on a test case. (Color figure online)

3.2 Registration Accuracy Assessment

Hologram-to-Phantom Registration. The global time required by the algorithm to compute the transformation matrix $\mathbf{T}_{CT}^{H2}$ and send it back to H2 was 0.26 ± 0.02 s, with a fitness of $92.93 \pm 3.91\%$ which measures the overlapping area between the cleaned PtC and the processed skin model, averaged over the 10 measurements. The median distance with interquartile range between $\boldsymbol{F}_{i,OT}$ and $\boldsymbol{H}_{i,OT}$ for the 4 markers, in the 10 repeated procedures, resulted in $1.25(0.65-1.72)$ mm, $1.75(0.98-2.42)$ mm, $1.35(0.41-1.83)$ mm, for the x, y, z coordinates in the OT space respectively (corresponding to the axial, sagittal and coronal plane of the phantom). The distances referred to each of the 4 markers in the 3 coordinates are reported in Fig. 5A. The average 3D Euclidean distance for all the markers over the 10 procedures resulted in 2.72 ± 0.67 mm. The point-to-point accuracy over the whole model as obtained from Eq. 2 showed a $RMSE$ of 3.19 ± 0.69 mm and 3.61 ± 1.13 mm for the face and ventricle surfaces respectively. Point-to-point distance maps between the surfaces are represented in Fig. 5C.

Ventriculostomy Procedure. Guided by the holographic system, a 42% higher accuracy was shown, on average. Euclidean target distances of blind vs. holographically-guided simulations are reported in Fig. 5B. In the blind procedure, the mean distance to the target was equal to 16.2 ± 3.48 mm, compared to a mean distance of 9.26 ± 3.27 mm for the hologram guided procedure, resulting in a statistically significant improvement on a paired t-test (p=0.001). Figure 5D graphically shows the final tip position in all the procedures done by the neurosurgeons compared to the FoM target in the ventricle.

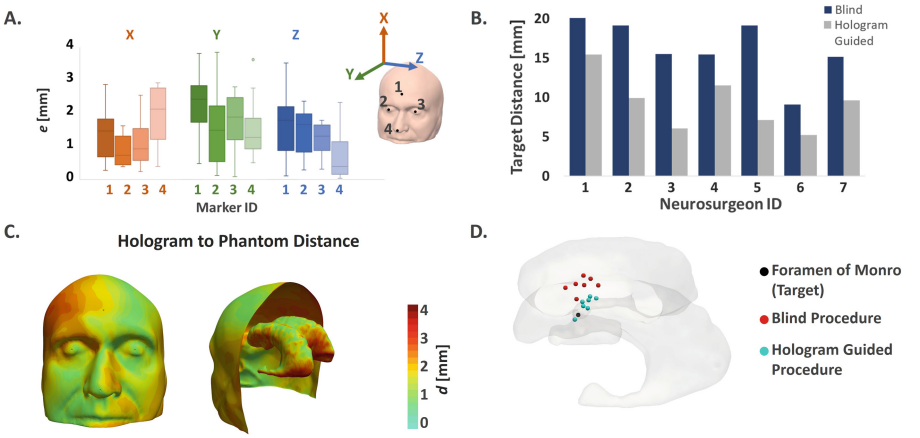

Fig. 5. Experimental results from evaluation tests. A: hologram-to-phantom accuracy evaluated on the 4 markers; B: quantitative targeting accuracy from the tests done by 7 neurosurgeons; C: hologram to phantom accuracy evaluated over the whole model surface; D: visualization of catheter tip positions and target from the EVD simulations.

4 Conclusions

The present study proposed a novel solution for supporting neurosurgeons during EVD procedures. Our system leverages a deep NN for automatic image segmentation and a markerless registration method based on a HMD depth sensor to align internal brain structures with the physical position of the patient. We quantitatively assessed the accuracy of our workflow at each of its steps, proving the added value to ventriculostomy procedures under experimental settings; adopting our technology, neurosurgeons targeting accuracy improved by 42%, on average. Of note, all the described steps require little or no manual intervention, and computations required globally less than 3 min, thus making our system suitable for emergency procedures where timing can be crucial. Our future efforts will focus on including an holographic navigation of the probe using

electromagnetic sensors and evaluate the accuracy of adding a further, independent, Azure Kinect (Microsoft, Redmond, WA) depth camera to achieve a more stable and robust point cloud acquisition. Moreover, a phantom reproducing the different resistance of the ventricles with respect to the brain will be adopted to simulate the surgical procedure in a more realistic way.

References

1. AlAzri, A., Mok, K., Chankowsky, J., Mullah, M., Marcoux, J.: Placement accuracy of external ventricular drain when comparing freehand insertion to neuronavigation guidance in severe traumatic brain injury. Acta Neurochir. **159**(8), 1399–1411 (2017). https://doi.org/10.1007/s00701-017-3201-5
2. Arun, K.S., Huang, T.S., Blostein, S.D.: Least-squares fitting of two 3-D point sets. IEEE Trans. Pattern Anal. Mach. Intell. **5**, 698–700 (1987)
3. Azimi, E., et al.: An interactive mixed reality platform for bedside surgical procedures. In: Martel, A.L., et al. (eds.) MICCAI 2020. LNCS, vol. 12263, pp. 65–75. Springer, Cham (2020). https://doi.org/10.1007/978-3-030-59716-0_7
4. Chen, Y., Medioni, G.: Object modelling by registration of multiple range images. Image Vis. Comput. **10**(3), 145–155 (1992)
5. van Doormaal, J.A., Fick, T., Ali, M., Köllen, M., van der Kuijp, V., van Doormaal, T.P.: Fully automatic adaptive meshing based segmentation of the ventricular system for augmented reality visualization and navigation. World Neurosurg. **156**, e9–e24 (2021)
6. Ester, M., et al.: A density-based algorithm for discovering clusters in large spatial databases with noise. In: Proceedings of the Second International Conference on Knowledge Discovery and Data Mining, vol. 96, pp. 226–231 (1996)
7. von Haxthausen, F., Chen, Y., Ernst, F.: Superimposing holograms on real world objects using Hololens 2 and its depth camera. Curr. Dir. Biomed. Eng. **7**(1), 111–115 (2021)
8. Katz, S., Tal, A., Basri, R.: Direct visibility of point sets. ACM Trans. Graph. **26**(3), 24-es (2007). https://doi.org/10.1145/1276377.1276407
9. Li, Y., et al.: A wearable mixed-reality holographic computer for guiding external ventricular drain insertion at the bedside. J. Neurosurg. **131**(5), 1599–1606 (2018)
10. Mahan, M., Spetzler, R.F., Nakaji, P.: Electromagnetic stereotactic navigation for external ventricular drain placement in the intensive care unit. J. Clin. Neurosci. **20**(12), 1718–1722 (2013)
11. Patrick, S., et al.: Comparison of gray values of cone-beam computed tomography with hounsfield units of multislice computed tomography: an in vitro study. Indian J. Dent. Res. **28**(1), 66 (2017)
12. Saitta, S., et al.: A deep learning-based and fully automated pipeline for thoracic aorta geometric analysis and planning for endovascular repair from computed tomography. J. Digit. Imaging **35**(2), 226–239 (2022)
13. Schneider, M., Kunz, C., Pal'a, A., Wirtz, C.R., Mathis-Ullrich, F., Hlaváč, M.: Augmented reality-assisted ventriculostomy. Neurosurg. Focus **50**(1), E16 (2021)
14. Shen, Dinggang, Shen, D., et al. (eds.): MICCAI 2019. LNCS, vol. 11764. Springer, Cham (2019). https://doi.org/10.1007/978-3-030-32239-7
15. Ungureanu, D., et al.: Hololens 2 research mode as a tool for computer vision research. arXiv preprint arXiv:2008.11239 (2020)

16. Wilson, T.J., Stetler, W.R., Al-Holou, W.N., Sullivan, S.E.: Comparison of the accuracy of ventricular catheter placement using freehand placement, ultrasonic guidance, and stereotactic neuronavigation. J. Neurosurg. **119**(1), 66–70 (2013)
17. Zhou, Q.-Y., Park, J., Koltun, V.: Fast global registration. In: Leibe, B., Matas, J., Sebe, N., Welling, M. (eds.) ECCV 2016. LNCS, vol. 9906, pp. 766–782. Springer, Cham (2016). https://doi.org/10.1007/978-3-319-46475-6_47
18. Zhou, Q.Y., Park, J., Koltun, V.: Open3D: a modern library for 3D data processing. arXiv preprint arXiv:1801.09847 (2018)